ISSN 2176-5480

22nd International Congress of Mechanical Engineering (COBEM 2013)
November 3-7, 2013, Ribeirão Preto, SP, Brazil
Copyright © 2013 by ABCM

VARICOSE SECONDARY INSTABILITIES CONTROL IN A GÖRTLER FLOW

Analice Costacurta Brandi
Faculdade de Ciências e Tecnologia
Universidade Estadual Paulista "Júlio de Mesquita Filho"
Rua Roberto Simonsen, 305
19060-900, Presidente Prudente - SP
analice@fct.unesp.br

Leandro Franco de Souza
Instituto de Ciências Matemáticas e de Computação
Universidade de São Paulo
Av. Trabalhador São Carlense, 400
13566-590, São Carlos - SP
lefraso@icmc.usp.br

Abstract. *Boundary layer flow over concave wall is subject to centrifugal instabilities, giving rise to primary instabilities that can seed longitudinal vortices, known as Görtler Vortices. Initially these vortices grow linearly and, when they reach a small amplitude, they begin to develop non-linearly until the saturation regime. During the non-linear phase, the vortices change the streamwise velocity distribution. The new velocity distribution has inflections in the spanwise and wall-normal directions. The inflections are susceptible to instabilities that give rise to secondary instabilities. In Görtler flow, the secondary instabilities can be sinuous and varicose modes. In this study, a Direct Numerical Simulation of this scenario is presented. Only the varicose mode is taken into account. The numerical scheme is based on high-order method: a 4th order Runge-Kutta scheme is adopted for time integration; compact high-order finite difference schemes are used to discretize the spatial derivatives in the streamwise and the wall-normal directions; a spectral method, based on Fourier transform is adopted to discretize the spanwise derivatives. The method is parallelized through domain decomposition in the streamwise direction adopting MPI libraries. The present study aims to control the transition scenario by using uniform suction. The results show that uniform suction is not effective in postponing the transition to turbulence. The energy of the unsteady modes reaches lower values with uniform suction, but the transition to turbulence remains almost in the same place.*

Keywords: *boundary layer flow, Görtler vortices, secondary instabilities, transition control*

1. INTRODUCTION

Turbulent flows are common in practical applications. There are a large number of situations in which transition to turbulence is important. That is the case for the flow over low Reynolds number turbine blades and laminar flow airfoils. The understanding of how transition takes place can help to predict and control transition to turbulence. Over recent years the body of knowledge on laminar flow stability and transition has increased due to the development of new experimental and numerical techniques as well as to advances in applied mathematical theories. However, there are many transition scenarios for which a physical explanation is still unknown, and transition location prediction remains a challenge in many engineering applications.

Many flows exhibit the following scenario: the flow starts out in an unstable laminar state; then a linear instability develops, and grows up to the point where nonlinear interactions finally lead to turbulence or another flow distribution different from the initial one. In many applications, it might be very interesting to delay this transition toward turbulence and, thus, to maintain the flow laminar. Consequently, a control system to control those instabilities is an initial objective.

Stationary streamwise vortices are found in the boundary layer over a concave wall – competition between centrifugal and pressure forces creates an instability leading to Görtler vortices (Hall (1982), Hall (1983), Floryan and Saric (1982), Swearingen and Blackwelder (1987), Saric (1994), Bottaro and Klingmann (1996)). The centrifugal instability mechanism is responsible for the development of counter-rotating vortices aligned in the streamwise direction, known as Görtler vortices. These vortices pump low momentum fluid away from the wall and high momentum fluid toward the wall forming upwash and downwash regions, respectively. This macroscopic redistribution of mass results in the development of mushroom type structures with strong inflectional velocity profiles in the wall-normal and streamwise directions. These inflectional velocity profiles are susceptible to high frequency secondary instability further downstream. Reviews on Görtler vortices with detailed description and theoretical background have been published by Hall (1990), Floryan (1991) and Saric (1994).

ISSN 2176-5480

Different stages of instability can be distinguished, depending on the state of the underlying base flow. The stage is denoted as primary if the unstable base flow is laminar (undisturbed), often initiating the transition process. For example, in a Blasius boundary layer the primary disturbance could be a purely two-dimensional wave inducing the growth of three-dimensional perturbations, or in Görtler flow large, primary steady vortices induce amplification of fluctuations in time. Such instabilities are called secondary instabilities. The strength of secondary amplification depends parametrically on the primary disturbance amplitude. Finally, tertiary and higher instabilities might occur.

Secondary instabilities are often associated with a weak non-linear stage of the flow, i.e. the flow field is modulated by a disturbance of small, but already non-linear amplitude. Thus, this stage is not related to a baseflow isolate property. The secondary disturbance development can be linear again, i.e. it depends parametrically on the primary disturbance and, thus, this ansatz is called weakly non-linear. Analysis of secondary instability is typically carried out in a frame of reference fixed with respect to the primary perturbation, allowing the assumption of periodicity in time and in the streamwise direction of the deformed base flow. For example, in case of a downstream-traveling Tollmien-Schlichting or Kelvin-Helmholtz (primary) wave, the secondary instability often belongs to the temporal instabilities. Since the secondary disturbance locks into the convection of the primary, one can think of a resonance.

The Görtler vortices are found to be subject to two types of secondary modes: the sinuous mode and the varicose mode, or a mix of them. In this paper we study the varicose secondary instabilities that generate structures known as horseshoe vortices. This type of instability has its origin in the upstream region, related to the derivative du/dy.

Typically, for a controlled transition process, the scenario can be determined by following the evolution of all observable disturbances without considering their role, while the mechanism can be determined only by a selective variation of the disturbance input and/or application of stability theories for the respective case, i.e. by identifying the importance of their contribution to the process.

It appears from the literature that a dynamic control by blowing and suction would be the most convenient means for controlling a boundary-layer flow (Floryan and Saric (1979), Myose and Blackwelder (1991), Myose and Blackwelder (1995)). Assuming that an optimal initial perturbation is present, in this paper, we focus on controlling the transition to turbulence through uniform suction at the wall.

2. FORMULATION

The Navier-Stokes equations written in the vorticity-velocity formulation are discretized using high-order finite-differences schemes and spectral approximations for the spatial derivatives and a 4^{th} order Runge-Kutta scheme for temporal discretization.

2.1 Governing equations

The governing equations are the incompressible unsteady Navier-Stokes equations with constant viscosity. Defining the vorticity as the negative curl of the velocity vector, and using the fact that both velocity and vorticity fields are solenoidal, one can obtain the following vorticity transport equation in each direction:

$$\frac{\partial\widetilde{\omega}_x}{\partial t}+\frac{\partial\widetilde{a}}{\partial y}-\frac{\partial\widetilde{b}}{\partial z}+\frac{Go^2}{\sqrt{Re}h}\frac{\partial\widetilde{d}}{\partial z}=\frac{1}{Re}\nabla^2\widetilde{\omega}_x, \tag{1}$$

$$\frac{\partial\widetilde{\omega}_y}{\partial t}+\frac{\partial\widetilde{c}}{\partial z}-\frac{\partial\widetilde{a}}{\partial x}=\frac{1}{Re}\nabla^2\widetilde{\omega}_y, \tag{2}$$

$$\frac{\partial\widetilde{\omega}_z}{\partial t}+\frac{\partial\widetilde{b}}{\partial x}-\frac{\partial\widetilde{c}}{\partial y}-\frac{Go^2}{\sqrt{Re}h}\frac{\partial\widetilde{d}}{\partial x}=\frac{1}{Re}\nabla^2\widetilde{\omega}_z, \tag{3}$$

where

$$\widetilde{a}=\widetilde{\omega}_x\widetilde{v}-\widetilde{\omega}_y\widetilde{u}, \tag{4}$$

$$\widetilde{b}=\widetilde{\omega}_z\widetilde{u}-\widetilde{\omega}_x\widetilde{w}, \tag{5}$$

$$\widetilde{c}=\widetilde{\omega}_y\widetilde{w}-\widetilde{\omega}_z\widetilde{v}, \tag{6}$$

$$\widetilde{d}=\widetilde{u}^2, \tag{7}$$

are the nonlinear terms resulting from convection, vortex stretching and vortex bending. The variables $(\widetilde{u},\widetilde{v},\widetilde{w},\widetilde{\omega}_x,\widetilde{\omega}_y,\widetilde{\omega}_z)$ are the velocity and vorticity components in the streamwise, wall-normal and spanwise directions, respectively; $\widetilde{t}$ is time. The Laplace operator is:

$$\nabla^2=\left(\frac{\partial^2}{\partial x^2}+\frac{\partial^2}{\partial y^2}+\frac{\partial^2}{\partial z^2}\right). \tag{8}$$

ISSN 2176-5480

The continuity equation is given by:

$$\frac{\partial \widetilde{u}}{\partial x} + \frac{\partial \widetilde{v}}{\partial y} + \frac{\partial \widetilde{w}}{\partial z} = 0. \tag{9}$$

The above equations are presented in a non-dimensional form. The reference length is a plate-characteristic length $\overline{L}$ and the reference velocity is the free stream velocity $\overline{U}_\infty$. The Reynolds number is given by $Re = \overline{U}_\infty \overline{L}/\overline{\nu}$, where $\overline{\nu}$ is the kinematic viscosity.

The Görtler number is given by $Go = (k_c\sqrt{Re})^{1/2}$. The terms $Go^2 \frac{\partial \widetilde{d}}{\partial x}/(\sqrt{Re}h)$ and $Go^2 \frac{\partial \widetilde{d}}{\partial z}/(\sqrt{Re}h)$ are the leading order curvature terms, where $h = 1 - k_c y$, $k_c = \overline{L}/\overline{R}$ is the wall curvature and $\overline{R}$ is the curvature radius.

Taking the vorticity definition and the mass conservation equation, one can obtain Poisson-type equations for each velocity component:

$$\frac{\partial^2 \widetilde{u}}{\partial x^2} + \frac{\partial^2 \widetilde{u}}{\partial z^2} = -\frac{\partial \widetilde{\omega}_y}{\partial z} - \frac{\partial^2 \widetilde{v}}{\partial x \partial y}, \tag{10}$$

$$\frac{\partial^2 \widetilde{v}}{\partial x^2} + \frac{\partial^2 \widetilde{v}}{\partial y^2} + \frac{\partial^2 \widetilde{v}}{\partial z^2} = -\frac{\partial \widetilde{\omega}_z}{\partial x} + \frac{\partial \widetilde{\omega}_x}{\partial z}, \tag{11}$$

$$\frac{\partial^2 \widetilde{w}}{\partial x^2} + \frac{\partial^2 \widetilde{w}}{\partial z^2} = \frac{\partial \widetilde{\omega}_y}{\partial x} - \frac{\partial^2 \widetilde{v}}{\partial y \partial z}. \tag{12}$$

2.2 Disturbance formulation

In the current study a disturbance formulation is adopted, i.e. the flow variables were decomposed in a base flow and a perturbation:

$$\widetilde{f} = f_b + f. \tag{13}$$

With such formulation, the stability analysis of any base flow (Blasius, Falkner-Skan, etc.), can be easily performed as both linear and nonlinear terms can be isolated. Some disadvantages of this formulation are the indirect access to the instantaneous flow variables and a higher memory use due to the larger number of variables.

The variables $\widetilde{f} = \{\widetilde{u}, \widetilde{v}, \widetilde{w}, \widetilde{\omega}_x, \widetilde{\omega}_y, \widetilde{\omega}_z\}$ are the total flow variables. The base flow is considered two-dimensional, therefore only u_b, v_b and ω_{z_b} are taken into account, where the index b indicates the base flow.

Introducing Eq. (13) in the equations (1) – (3) and (10) – (12) and subtracting the base flow, the equations for the perturbations result in:

$$\frac{\partial \omega_x}{\partial t} + \frac{\partial a}{\partial y} - \frac{\partial b}{\partial z} + \frac{Go^2}{\sqrt{Re}h}\frac{\partial d}{\partial z} = \frac{1}{Re}\nabla^2 \omega_x, \tag{14}$$

$$\frac{\partial \omega_y}{\partial t} + \frac{\partial c}{\partial z} - \frac{\partial a}{\partial x} = \frac{1}{Re}\nabla^2 \omega_y, \tag{15}$$

$$\frac{\partial \omega_z}{\partial t} + \frac{\partial b}{\partial x} - \frac{\partial c}{\partial y} - \frac{Go^2}{\sqrt{Re}h}\frac{\partial d}{\partial x} = \frac{1}{Re}\nabla^2 \omega_z, \tag{16}$$

$$\frac{\partial^2 u}{\partial x^2} + \frac{\partial^2 u}{\partial z^2} = -\frac{\partial \omega_y}{\partial z} - \frac{\partial^2 v}{\partial x \partial y}, \tag{17}$$

$$\frac{\partial^2 v}{\partial x^2} + \frac{\partial^2 v}{\partial y^2} + \frac{\partial^2 v}{\partial z^2} = -\frac{\partial \omega_z}{\partial x} + \frac{\partial \omega_x}{\partial z}, \tag{18}$$

$$\frac{\partial^2 w}{\partial x^2} + \frac{\partial^2 w}{\partial z^2} = \frac{\partial \omega_y}{\partial x} - \frac{\partial^2 v}{\partial y \partial z}, \tag{19}$$

where the nonlinear terms a, b, c and d are:

$$a = \omega_x(v_b + v) - \omega_y(u_b + u), \tag{20}$$

$$b = (\omega_{z_b} + \omega_z)(u_b + u) - \omega_x w, \tag{21}$$

$$c = \omega_y w - (\omega_{z_b} + \omega_z)(v_b + v), \tag{22}$$

$$d = 2u_b u + u^2. \tag{23}$$

ISSN 2176-5480

3. NUMERICAL METHOD

3.1 Discretization of field equations

The flow is assumed to be periodic in the spanwise direction. Therefore, the flow field can be expanded in Fourier series with K spanwise Fourier modes:

$$f(x,y,z,t) = \sum_{k=0}^{K} F_k(x,y,t)e^{(i\beta_k z)}, \tag{24}$$

where $f = u, v, w, \omega_x, \omega_y, \omega_z, a, b, c, d$; $F_k = U_k, V_k, W_k, \Omega_{x_k}, \Omega_{y_k}, \Omega_{z_k}, A_k, B_k, C_k, D_k$; and β_k is the spanwise wavenumber given by $\beta_k = 2\pi k/\lambda_z$, and λ_z is the spanwise wavelength of the fundamental spanwise Fourier mode, and $i = \sqrt{-1}$. Note that the F_k may be fully complex, i.e. non-symmetric three-dimensional disturbance fields can be computed.

Substituting the Fourier transforms (Eq. 24) in the vorticity transport equations (14) – (16) and in the velocity Poisson equations (17) – (19) yield the governing equations in the Fourier space:

$$\frac{\partial \Omega_{x_k}}{\partial t} + \frac{\partial A_k}{\partial y} - \beta_k B_k - \frac{Go^2}{\sqrt{Re}}\frac{\beta_k(D_k^2)}{h} = \frac{1}{Re}\nabla_k^2 \Omega_{x_k}, \tag{25}$$

$$\frac{\partial \Omega_{y_k}}{\partial t} + \beta_k C_k - \frac{\partial A_k}{\partial x} = \frac{1}{Re}\nabla_k^2 \Omega_{y_k}, \tag{26}$$

$$\frac{\partial \Omega_{z_k}}{\partial t} + \frac{\partial B_k}{\partial x} + \frac{\partial C_k}{\partial y} - \frac{Go^2}{\sqrt{Re}h}\frac{\partial (D_k^2)}{\partial x} = \frac{1}{Re}\nabla_k^2 \Omega_{z_k}, \tag{27}$$

$$\frac{\partial^2 U_k}{\partial x^2} - \beta_k^2 U_k = -\beta_k \Omega_{y_k} - \frac{\partial^2 V_k}{\partial x \partial y}, \tag{28}$$

$$\frac{\partial^2 V_k}{\partial x^2} + \frac{\partial^2 V_k}{\partial y^2} - \beta_k^2 V_k = -\frac{\partial \Omega_{z_k}}{\partial x} + \beta_k \Omega_{x_k}, \tag{29}$$

$$\frac{\partial^2 W_k}{\partial x^2} - \beta_k^2 W_k = \frac{\partial \Omega_{y_k}}{\partial x} + \beta_k \frac{\partial V_k}{\partial y}, \tag{30}$$

where $\nabla_k^2 = \left(\frac{\partial^2}{\partial x^2} + \frac{\partial^2}{\partial y^2} - \beta_k^2\right)$.

The Eq. (25) – (30) are solved numerically in the domain as shown schematically in Fig. 1. The calculations are done on an orthogonal uniform grid, parallel to the wall. The fluid enters the computational domain at $x = x_0$ and exits at the outflow boundary $x = x_{max}$. Steady disturbances are introduced into the flow field using spanwise suction and blowing in a disturbance strip at the wall. This strip is located between x_1 and x_2. Another disturbance strip is used to introduce unsteady disturbances located in the region where the vortices are already nonlinear. These unsteady disturbances are used to study the secondary instabilities. In the region located between x_3 and x_4 a buffer domain technique, from Kloker *et al.* (1993), is implemented in order to avoid wave reflections at the outflow boundary. In these simulations a Blasius boundary layer is used as the base flow.

The time derivatives in the vorticity transport equations are discretized with a classical 4^{th} order Runge-Kutta integration scheme (Ferziger and Peric (1997)). The spatial derivatives are calculated using a high-order compact finite difference-schemes (Souza *et al.* (2005); Souza (2003); Lele (1992); Kloker (1998)). The V-Poisson equation – Eq. (29) – is solved using a multigrid Full Approximation Scheme (FAS) (Stüben and Trottenberg (1981)). A V-cycle working with 4 grids is implemented. The code adopted is parallelized using domain decomposition in the streamwise direction.

3.2 Boundary conditions

At the wall ($y = 0$), a no-slip condition is imposed to both the streamwise (U_k) and the spanwise (W_k) velocity components. The wall-normal velocity component at the wall (V_k) is specified at the suction and blowing strip region between x_1 and x_2, where the disturbances are introduced. Away from the disturbance generator, this velocity component is set to zero. The function used for the wall-normal velocity V_1 at the disturbance generator is:

$$V_1(x,0,t) = A_1 \sin^3(\epsilon) \quad \text{for} \quad l_1 \leq l \leq l_2, \tag{31}$$

where $\epsilon = \pi(l - l_1)/(l_2 - l_1)$ and A_1 is a real constant chosen to adjust the steady disturbance amplitude. The variable l indicates the grid point location x_l in the streamwise direction, and points l_1 and l_2 correspond to x_1 and x_2 respectively.

ISSN 2176-5480

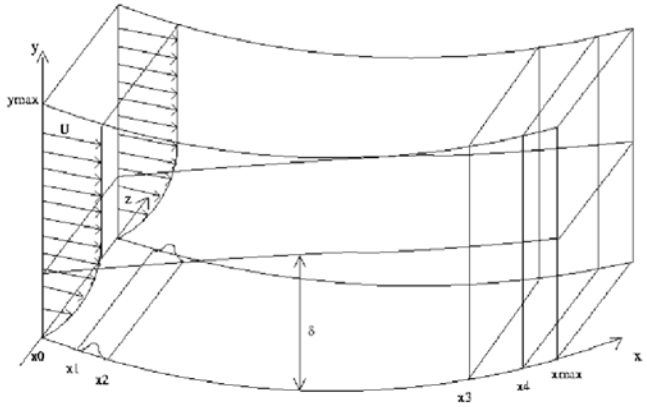

Figure 1. Solution domain.

The unsteady disturbances, used to study the secondary instabilities, are also introduced at the wall. It consists in introducing a slot at the wall, $x_{fs} \leq x \leq x_{ls}$, where x_{fs} and x_{ls} are, respectively, the first and the last x-position of the unsteady disturbance strip. The function used for velocity V is:

$$V_1(x, 0, t) = f_1(x) A_2 \sin(\omega_t t) \qquad \text{for} \qquad x_i \leq x \leq x_f. \tag{32}$$

A_2 is a real constant and can be chosen to adjust the unsteady disturbances amplitude; ω_t is the dimensionless frequency. The adopted function $f_1(x)$ is a fifth-order function, proposed by Zhang and Fasel (1999). This function is used in order to make sure that, at $y = 0$, the vertical velocity components, its first and second derivatives do not have a discontinuity going in and out of the suction and blowing region.

At the inflow boundary ($x = x_0$), the velocity and the vorticity components are specified based on the Blasius boundary-layer solution. At the outflow boundary ($x = x_{max}$), the second derivatives with respect to the streamwise direction of the velocity and vorticity components are set to zero. At the upper boundary ($y = y_{max}$) the flow is considered non rotational. This is satisfied by setting all vorticity components and their derivatives to zero. The wall-normal velocity component at the upper boundary is calculated using the condition:

$$\frac{\partial V_k}{\partial y}|_{x, y_{max}, t} = 0.. \tag{33}$$

In addition, at the wall, the condition $\partial V_k / \partial y = 0$ is imposed in the solution of the U_k velocity Poisson equation (Eq. 28), to ensure the mass conservation. The equations used for evaluating the vorticity components at the wall are:

$$\frac{\partial^2 \Omega_{x_k}}{\partial x^2} - \beta_k^2 \Omega_{x_k} = -\frac{\partial^2 \Omega_{y_k}}{\partial x \partial y} - \beta_k \nabla_k^2 V_k, \tag{34}$$

$$\frac{\partial \Omega_{z_k}}{\partial x} = \beta_k \Omega_{x_k} - \nabla_k^2 V_k. \tag{35}$$

A damping zone is defined near the outflow boundary, in which all the disturbances are gradually damped down to zero (Kloker *et al.* (1993)). This technique is used to avoid reflections in the outflow boundary. Meitz and Fasel (2000) adopted a fifth-order polynomial, and the same function is used in the present model. The basic idea is to multiply the vorticity components by a ramp function $f_2(x)$ after each sub-step of the integration method. Using this technique, the vorticity components are taken as:

$$\Omega_k(x, y, t) = f_2(x) \Omega_k^*(x, y, t), \tag{36}$$

where $\Omega_k^*(x, y, t)$ is the disturbance vorticity component that results from the Runge-Kutta integration and $f_2(x)$ is a ramp function that goes smoothly from 1 to 0. The implemented function is:

$$f_2(x) = f(\epsilon) = 1 - 6\epsilon^5 + 15\epsilon^4 - 10\epsilon^3, \tag{37}$$

where $\epsilon = (l - l_3)/(l_4 - l_3)$ for $l_3 \leq l \leq l_4$. The points l_3 and l_4 correspond, respectively, to the positions x_3 and x_4 in the streamwise direction. To ensure good numerical results and efficiency, a minimum distance between x_3 and x_4 and between x_4 and the end of the domain x_{max} were studied. In the following simulations, the zones had 30 grid points in each region.

ISSN 2176-5480

Another buffer domain, located near the inflow boundary, was also implemented in the code. As pointed out by Meitz (1996) in simulations involving streamwise vortices, reflections due to the vortices at the inflow can contaminate the numerical solution. The damping function is similar to the one used for the outflow boundary:

$$f_2(x) = f(\epsilon) = 6\epsilon^5 - 15\epsilon^4 + 10\epsilon^3, \tag{38}$$

where ϵ is $\epsilon = (l-1)/(l_1-1)$ for the range $1 \leq l \leq l_1$. All the vorticity components are multiplied by this function in this region.

4. NUMERICAL SIMULATIONS AND RESULTS

The parameters used were those of the experiment of Swearingen and Blackwelder (1987). They considered a boundary layer on a concave plate with $\bar{R} = 3.20$ m and free-stream velocity $\bar{U}_\infty = 5$ m/s. The numerical domain starts at $x_0 = 100$ mm downstream the leading edge, which corresponds to a boundary-layer thickness parameter $\delta = \sqrt{\bar{\nu}\bar{x}_0/\bar{U}_\infty} = 5.477\times10^{-2}$ cm, a Görtler number $Go = 2.38859$ and a Reynolds number $Re = 33124$. In the experiment, the average spanwise wavelength was $\bar{\lambda}_z = 18$ mm, which corresponds to a non-dimensional wavenumber of $\beta = 34.90$. This corresponds to a wavelength parameter for the fundamental Fourier mode, given by $\Lambda_f = (\bar{U}_\infty\bar{\lambda}_z/\bar{\nu})(\bar{\lambda}_z/\bar{R})^{1/2}$, of $\Lambda_f = 450$. The reference length used is $\bar{L} = 10$ cm. The number of grid points used was 2329 and 201 in the streamwise and the wall-normal directions, respectively. The non-dimensional uniform grid spacing is 5.00×10^{-3} in the streamwise. In the wall-normal direction a stretching grid was adopted with the first distance equal 8×10^{-4} and a constant stretching factor of 1%. The disturbance-strip location was $1.6 \leq x \leq 2.6$. Twenty one Fourier modes were used in the simulation. Test runs with a smaller grid spacing and larger number of Fourier modes indicated that the solutions were grid independent.

The verification and the validation of the code adopted in the present paper can be found in Souza *et al.* (2004); Malatesta *et al.* (2013). Initially the flow is simulated only with steady disturbances, that give birth to the Görtler vortices. The domain in the streamwise direction has enough length to let the Vortices appear, develop linearly, non-linearly and finally, reach the saturation region. In the saturated flow the non-steady disturbances are introduced with different frequencies, from 20 Hz to 320 Hz, with steps of 20 Hz, in order to verify the receptivity and the secondary instabilities in the flow field. These disturbances are introduced in a region where the flow is already saturated, using suction and blowing at the wall. The amplitude of each disturbance is below 10^{-4}. It was made a Fourier analysis of each frequency mode (analyzing the streamwise velocity), verifying where the maximum disturbance value of each frequency mode in each $y \times z$ plane is, namely $U_{max}(y,z)$. In Fig. 2 it can be observed that the frequency corresponding to 180 Hz has the maximum growth rate, and that in the unsteady disturbances saturation region the 20 Hz has the maximum value.

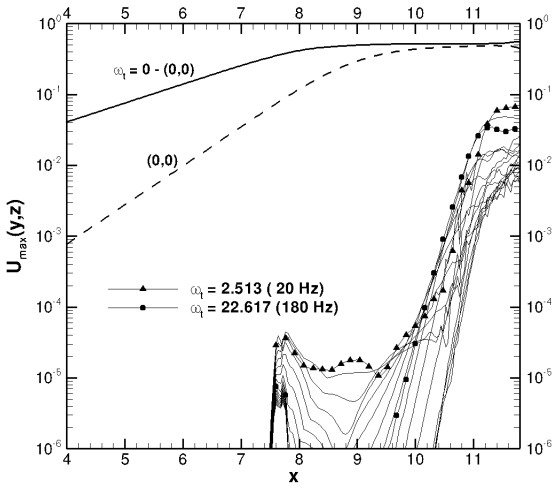

Figure 2. Maximum streamwise velocity disturbance over $y \times z$ plane in the streamwise direction. No suction case.

In order to verify the effect of uniform suction in the secondary instabilities development, it was introduced a slot at the wall, from $x = 8.5$ to $x = 11.7$. For the suction at the wall at this slot three values were tested: 1×10^{-4} case, 5×10^{-4} case, 1×10^{-3} case. These values are a percentage of the $\overline{U}_\infty$ velocity. In each case the streamwise development of $U_{max}(y,z)$ was also analyzed.

Figure 3 shows $U_{max}(y,z)$ for the case with uniform suction of 1×10^{-4}. It can be observed that the uniform suction effect is very small and no significant difference was observed compared to no suction case (Fig. 2).

Multiplying the suction adopted in the last case by a factor of 5, in the 5×10^{-4} case, and analyzing the evolution of $U_{max}(y,z)$ in the streamwise direction similar conclusion can be reached. The difference between the cases can be

ISSN 2176-5480

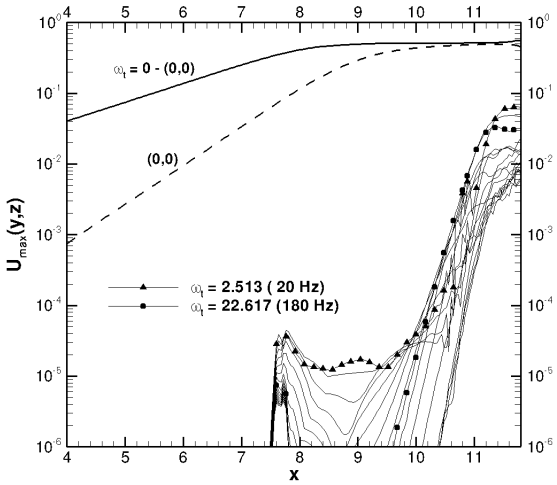

Figure 3. Maximum streamwise velocity disturbance over $y \times z$ plane in the streamwise direction. Uniform suction of 1×10^{-4} case.

observed by a small amount of amplitude of each mode in the saturation region, showing just a small delay in the transition process.

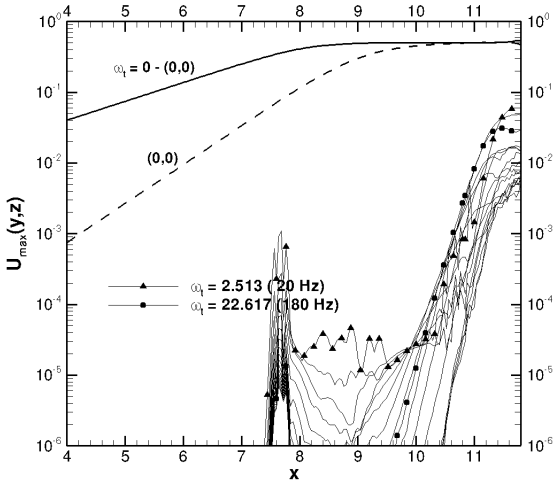

Figure 4. Maximum streamwise velocity disturbance over $y \times z$ plane in the streamwise direction. Uniform suction of 5×10^{-4} case.

The last case was simulated with an uniform suction of 1×10^{-3}, or 0.1 % of the streamwise velocity out of the boundary layer. Figure 5 shows the results for $U_{max}(y, z)$. It can also be observed a very small delay in the transition process and the amplitude of the unsteady modes is a bit smaller than the no-suction case.

The vortical structures in the instantaneous flow are visualized by Q iso-surfaces to allow the identification of coherent vortices. Details of this vortex identification technique are given in Dubief and Delvayre (2000). Figure 6 shows a sequence in time of Q iso-surfaces with a value of $Q = 0.5$, for the case with uniform suction of 5×10^{-4}. Two spanwise wavelengths are shown and the center of the figure in the spanwise direction corresponds to an upwash region. Each figure is $\Delta t = T/8$ apart from the previous figure giving a complete sequence over one period. In all figures the Görtler vortices can be seen as four longitudinal rolls up to $x \approx 10.00$. The horseshoe structures typical of even secondary-mode instability can be clearly seen. In the sequence of figures it can be observed that: (a) initially the background disturbances are first noticed; (b) these disturbances are convected downstream as their amplitudes grow; the next two figures (c) and (d) in the sequence show that the horseshoe vortices are convected downstream and other horseshoe vortices are formed behind the first one; Figures (e) and (f) show that these structures are convected and deformed downstream. In the last two figures of the sequence, structures with high frequencies appear in a region where the amplitudes of all modes reach saturation. These figures show that the secondary instabilities, that give rise to the horseshoe vortices are still present, and that the uniform suction did not suppress the transition to turbulence.

ISSN 2176-5480

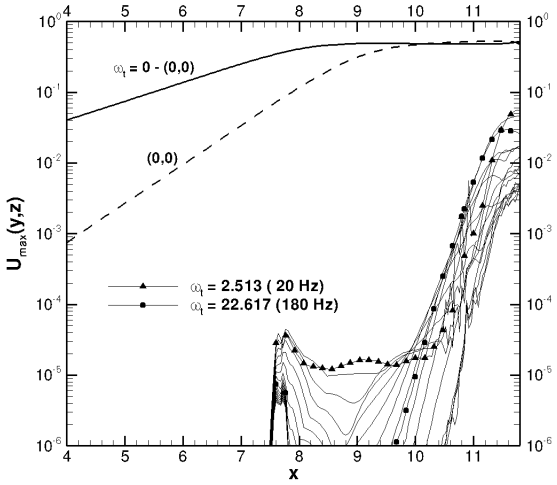

Figure 5. Maximum streamwise velocity disturbance over $y \times z$ plane in the streamwise direction. Uniform suction of 1×10^{-3} case.

5. CONCLUSIONS

In this paper is presented a Direct Numerical Simulation performed to study the effect of uniform suction in the laminar-turbulent transition control. The boundary layer flow over a concave wall was initially disturbed with steady disturbances giving rise to a Görtler flow. Unsteady disturbances were introduced in the flow field to verify the development of secondary instabilities. This transitional flow was used to verify the effect of uniform suction at the wall. The aim was to postpone the laminar-turbulent transition.

The results were obtained with 3 values of suction: 1×10^{-4} case, 5×10^{-4} case, 1×10^{-3} case. These values represent a percentage of the $\overline{U}_\infty$ velocity. In each case the streamwise development of $U_{max}(y, z)$ was analyzed. The results showed that, with the values used for suction, only a small delay was obtained. Further work will deal with localized suction and blowing to verify their effects in this process.

6. ACKNOWLEDGEMENTS

The authors acknowledge the financial support received from FAPESP.

7. REFERENCES

Bottaro, A. and Klingmann, B.B., 1996. "On the linear breakdown of Görtler vortices". *Eur. J. Mech. B / Fluids*, Vol. **15**, pp. 301–330.

Dubief, Y. and Delvayre, F., 2000. "On coherent-vortex identification in turbulence". *J. of Turbulence*, Vol. **011**, pp. 1–22.

Ferziger, J.H. and Peric, M., 1997. *Computational Methods for Fluid Dynamics*. Springer-Verlag Berlin Heidelberg New York.

Floryan, J.M., 1991. "On the Görtler instability of boundary layers". *Prog. Aerospace Sci.*, Vol. **28**, pp. 235–271.

Floryan, J.M. and Saric, W.S., 1979. "Stability of Görtler vortices in boundary layers with suction". *AIAA J.*, pp. Paper 79–1479.

Floryan, J.M. and Saric, W.S., 1982. "Stability of Görtler vortices in boundary layers". *AIAA J.*, Vol. **20**, No. 3, pp. 316–324.

Hall, P., 1982. "Taylor-Görtler vortices in fully developed or boundary layer flows: linear theory". *J. Fluid Mech.*, Vol. **124**, pp. 475–494.

Hall, P., 1983. "The linear development of gortler vortices in growing boundary-layers". *J. Fluid Mech.*, Vol. **130**, pp. 41–58.

Hall, P., 1990. "Görtler vortices in growing boundary layer: the leading edge receptivity problem, linear growth and the nonlinear breakdown stage". *Mathematika*, Vol. **37**, No. 74, pp. 151–189.

Kloker, M., 1998. "A robust high-resolution split-type compact fd scheme for spatial direct numerical simulation of boundary-layer transition". *Applied Scientific Research*, Vol. **59**, pp. 353–377.

Kloker, M., Konzelmann, U. and Fasel, H.F., 1993. "Outflow boundary conditions for spatial navier-stokes simulations of transition boundary layers". *AIAA Journal*, Vol. **31**, pp. 620–628.

Lele, S., 1992. "Compact finite difference schemes with spectral-like resolution". *J. Comput. Phys.*, Vol. **103**, pp. 16–42.

ISSN 2176-5480

Malatesta, V., Souza, L.F. and Liu, J.T.C., 2013. "Influence of Görtler vortices spanwise wavelenght on heat transfer rates". *Computational Thermal Sciences*, Vol. 5, No. 5. Accepted.

Meitz, H.L., 1996. *Numerical Investigation of Suction in a Trasitional Flat-Plate Boundary Layer*. Ph.D. thesis, The University of Arizona.

Meitz, H.L. and Fasel, H.F., 2000. "A compact-difference scheme for the navier-stokes equations in vorticity-velocity formulation." *J. Comp. Phys.*, Vol. **157**, pp. 371–403.

Myose, R.Y. and Blackwelder, R.F., 1991. "Controlling the spacing of streamwise vortices on concave walls". *AIAA Journal*, Vol. 29, No. 11, pp. 1901–1905.

Myose, R.Y. and Blackwelder, R.F., 1995. "Control of streamwise vortices using selective suction". *AIAA Journal*, Vol. 33, No. 6, pp. 1076–1080.

Saric, W.S., 1994. "Görtler vortices". *Ann. Rev. Fluid Mech.*, Vol. **26**, pp. 379–409.

Souza, L.F., 2003. *Instabilidade Centrífuga e transição para turbulência em Escoamentos Laminares Sobre Superfícies Côncavas*. Ph.D. thesis, Instituto Tecnológico de Aeronáutica.

Souza, L.F., Mendonça, M.T., de Medeiros, M.A.F. and Kloker, M., 2004. "Seeding of Görtler vortices through a suction and blowing strip". *Journal of the Brazilian Society of Mechanical Sciences*, Vol. XXVI, pp. 269–279.

Souza, L.F., Mendonça, M.T. and Medeiros, M.A.F., 2005. "The advantages of using high-order finite differences schemes in laminar-turbulent transition studies". *International Journal for Numerical Methods in Fluids*, Vol. **48**, pp. 565–592.

Stüben, K. and Trottenberg, U., 1981. *Nonlinear multigrid methods, the full approximation scheme*, Köln-Porz, chapter 5, pp. 58–71.

Swearingen, J.D. and Blackwelder, R.F., 1987. "The growth and breakdown of streamwise vortices in the presence of a wall". *J. Fluid Mech.*, Vol. **182**, pp. 255–290.

Zhang, H. and Fasel, H.F., 1999. "Spatial direct numerical simulation of Görtler vortices". In *AIAA Fluid Dynamics Conference*. Norfolk, USA.

8. RESPONSIBILITY NOTICE

The authors are the only responsible for the printed material included in this paper.

ISSN 2176-5480

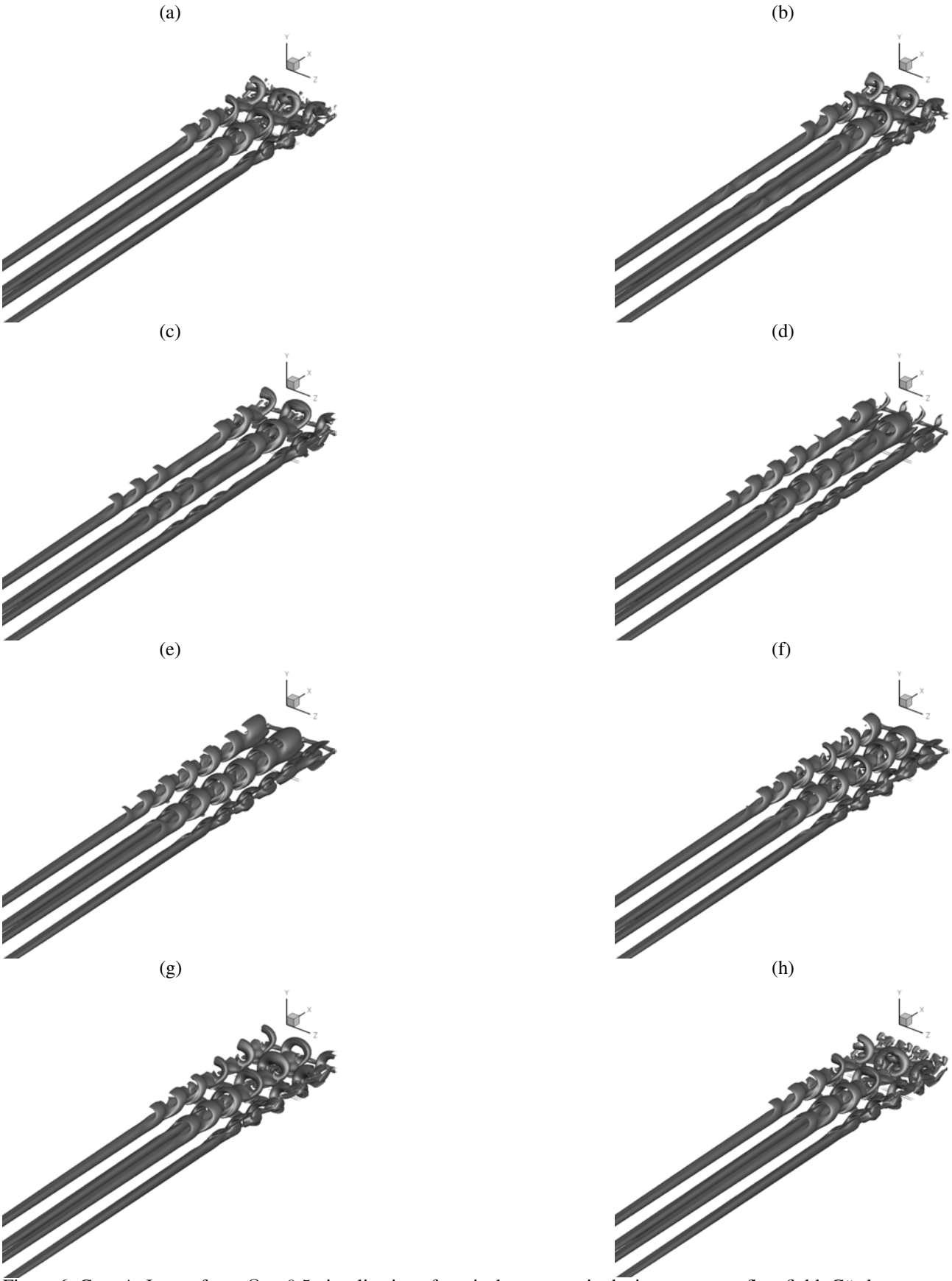

Figure 6. Case A: Iso-surfaces $Q = 0.5$ visualization of vortical structures in the instantaneous flow field. Görtler-vortex-mode plus periodic background pulses. (a) t/T=0, (b) t/T=1/8, (c) t/T=2/8, (d) t/T=3/8, (e) t/T=4/8, (f) t/T=5/8, (g) t/T=6/8, (h) t/T=7/8. T is the period for $\omega_t = 2.513$ (20 Hz). Two spanwise wavelengths are shown.